Cell, Vol. 123, 507–519, November 4, 2005, Copyright ©2005 by Elsevier Inc. DOI 10.1016/j.cell.2005.08.031

Exploration of the Function and Organization of the Yeast Early Secretory Pathway through an Epistatic Miniarray Profile

Maya Schuldiner,[1] Sean R. Collins,[1] Natalie J. Thompson,[2] Vladimir Denic,[1] Arunashree Bhamidipati,[1] Thanuja Punna,[2] Jan Ihmels,[1] Brenda Andrews,[2,3] Charles Boone,[2,3] Jack F. Greenblatt,[2,3] Jonathan S. Weissman,[1,*] and Nevan J. Krogan[2,3,4]

[1]Howard Hughes Medical Institute
Department of Cellular and Molecular Pharmacology
University of California, San Francisco
San Francisco, California 94143

[2]Banting and Best Department of Medical Research
University of Toronto
112 College Street
Toronto, Ontario M5G 1L6
Canada

[3]Department of Medical Genetics and Microbiology
University of Toronto
1 Kings College Circle
Toronto, Ontario M5S 1A8
Canada

Summary

We present a strategy for generating and analyzing comprehensive genetic-interaction maps, termed E-MAPs (*e*pistatic *minia**rray* *p*rofiles), comprising quantitative measures of aggravating or alleviating interactions between gene pairs. Crucial to the interpretation of E-MAPs is their high-density nature made possible by focusing on logically connected gene subsets and including essential genes. Described here is the analysis of an E-MAP of genes acting in the yeast early secretory pathway. Hierarchical clustering, together with novel analytical strategies and experimental verification, revealed or clarified the role of many proteins involved in extensively studied processes such as sphingolipid metabolism and retention of HDEL proteins. At a broader level, analysis of the E-MAP delineated pathway organization and components of physical complexes and illustrated the interconnection between the various secretory processes. Extension of this strategy to other logically connected gene subsets in yeast and higher eukaryotes should provide critical insights into the functional/organizational principles of biological systems.**

Introduction

A comprehensive understanding of cellular life requires a multitiered description of its organizing principles. This involves cataloging the molecular activities of individual proteins, obtaining information on how proteins are organized into pathways and complexes, and describing how the different biological processes influence each other. A variety of genomic and proteomic strategies for systematically obtaining such information exist, including identification of genes that are coregulated by DNA microarrays (Eisen et al., 1998; Hughes et al., 2000) and definition of physical complexes by affinity purification (Gavin et al., 2002; Ho et al., 2002) or two-hybrid studies (Ito et al., 2001; Uetz et al., 2000). An alternate approach for exploring function is to look for genetic interactions. In *Saccharomyces cerevisiae*, this has been accomplished in a systematic manner by exploiting the library of deletion strains to qualitatively identify pairs of gene deletions that lead to a synthetic sick/lethal (SSL) phenotype (Pan et al., 2004; Tong et al., 2001, 2004). The information collected using this approach is highly complementary to transcriptional and physical interaction data since it identifies processes that act in parallel to support viability. However, because SSL interactions are most often found between genes involved in distinct processes (Kelley and Ideker, 2005), interpretation of the cause and significance of such interactions is often challenging.

SSL analysis, in fact, represents only a specific case of the broader phenomenon of epistasis in which the phenotypic consequence of altering one gene is modulated by the presence or absence of a second one. This includes both negative (aggravating) interactions detected in SSL studies as well as positive ones such as buffering interactions where the cost of eliminating one gene is mitigated by the loss of a second one and true suppressor interactions in which the double mutant is healthier than the sickest single mutant. Theoretical considerations suggest that comprehensive and quantitative epistatic data could provide detailed information not only on protein function but on higher levels of cellular organization (Segre et al., 2005). However, interpretation of such data requires high-density maps since much of the information is distributed across patterns of interactions (Segre et al., 2005). Moreover, the ability to measure positive interactions provides a critical supplement to SSL (which typically connects distinct processes) as genes that act together in a single complex or pathway will often have buffering interactions with each other. Thus, the quality and completeness of a genetic-interaction map will determine the precision by which the function and organization of proteins can be resolved.

More broadly, knowledge of the spectrum of epistatic relationships is crucial for analyzing the manifestation of quantitative traits, for guiding efforts to tailor drug treatments to an individual's genetic makeup, and for developing rational strategies for drug-combination therapies. Finally, central features of evolutionary biology, including maintenance of genetic variability, sexual reproduction, and speciation, are dependent on the structure of genetic interactions (Elena and Lenski, 1997; Phillips et al., 2000).

Efforts to construct high-density, quantitative epistatic interaction maps face three major technical challenges. First, the number of gene pairs is enormous

*Correspondence: weissman@cmp.ucsf.edu
[4]Present address: Department of Biochemistry and Biophysics, University of California, San Francisco, San Francisco, California 94143.

(nearly 20 million in *S. cerevisiae*) and the density of interactions is low (estimated [Tong et al., 2004] to be 1 in 200 for SSL pairs involving nonessential genes). This puts a tremendous demand on the quantity and quality of data needed to generate a complete, whole-cell network of genetic interactions. However, the spatial and functional compartmentalization of cells results in "neighborhood clustering" in which there is a far higher density of genetic interactions between genes encoding colocalized and coregulated proteins (Huh et al., 2003; Tong et al., 2004). Because the number of possible interactions scales as the square of the number of genes, screening for genetic interactions within a limited, predominantly self-contained gene subset greatly increases the density of hits (and thus the signal-to-noise ratio) while drastically reducing the number of gene pairs that need to be tested.

The second obstacle is that detection of positive interactions requires quantitative comparisons between the growth of double and single mutants. This can be far more challenging than detection of SSL interactions, which involves only the identification of inviable double mutants. The collection of high-density interaction data enables an elegant solution to this challenge. Because it provides a large data set for each gene, it allows precise comparisons between the observed viability of a given double mutant and that typical of other double mutants involving each of the two genes.

The final important limitation to the construction of comprehensive epistatic maps is that there is no simple method for generating hypomorphic alleles of essential genes. However, essential proteins are most likely to be conserved across phyla and to play central roles in cellular function (Giaever et al., 2002). In order to include genes essential for cell viability, we have developed a simple strategy for generating such alleles, termed DAmP (*d*ecreased *a*bundance by *m*RNA *p*erturbation), which enables large-scale genetic and functional analyses.

Based on the above considerations, we present a strategy for generating comprehensive descriptions, termed E-MAPs (epistatic *m*iniarray *p*rofiles), of genetic interactions between logically connected subsets of genes. We further describe the construction and analysis of an E-MAP of genes acting in the yeast early secretory pathway (ESP). We chose this particular subset of proteins because the pathway is spatially restricted and its central functions (e.g., lipid biosynthesis and translocation, folding, processing, and trafficking of secreted proteins) are highly conserved and crucial to many metazoan processes, including development and the function of the immune, neuronal, and endocrine systems.

Results and Discussion

DAmP: A General Approach for Creating Hypomorphic Alleles

To enable the systematic analysis of the essential genes of *S. cerevisiae*, we developed a robust and efficient technique, DAmP, for generating hypomorphic alleles. DAmP utilizes simple, PCR-based homologous recombination to disrupt the natural 3′UTR by insertion of an antibiotic-resistance marker, thus greatly destabilizing the corresponding messages (Muhlrad and Parker, 1999). The DAmP strategy yields proteins under their natural transcriptional regulation but at substantially reduced levels (see Table S1 in the Supplemental Data available with this article online). For the large majority of essential genes, in the absence of additional stress, the DAmP alleles are expressed at levels sufficient to support viability. This approach complements promoter replacement alleles (Mnaimneh et al., 2004), which often are not well suited for large-scale genetic-interaction studies due to difficulties in achieving intermediate expression levels (N.J.K. and J.F.G., unpublished data).

To evaluate the utility of DAmP alleles, we focused on five well-characterized, essential proteins of the ESP. First, we showed that DAmP alleles of two genes, *SEC62* and *SEC63*, that encode components of the translocon have greatly reduced protein levels compared to wild-type (Figure 1A, top panel). These alleles show strong aggravating interactions with genes encoding seven nonessential components of the translocation process (Figure 1A, bottom panel). Second, we show that the DAmP strain of the major ER chaperone and HSP70 homolog, *KAR2*, has an approximately 2-fold reduction in protein level (Figure 1B, top left panel). Here, the relatively small decrease results from induction of the unfolded protein response (UPR) (Figure 1B, bottom panel), an ESP-specific stress response that induces *KAR2* transcription (Patil and Walter, 2001). This leads to a synthetic-lethal genetic interaction between a *kar2*-DAmP strain and a *Δire1* strain that cannot induce the UPR (Figure 1B, top right panel). Finally, we used the DAmP method on *PDI* and *ERO1*, which together are responsible for promoting disulfide formation (Tu and Weissman, 2004). Pdi1p levels were greatly reduced (Figure 1C, top panel), and both strains showed the strong sensitivity to the reducing agent dithiothreitol (DTT) (Figure 1C, bottom panels) characteristic of strains with reduced Pdi1p or Ero1p activity (Tu and Weissman, 2004). The ease of implementation and robustness of the DAmP approach (illustrated here and below) now make the essential part of the yeast genome readily accessible to the type of comprehensive chemical sensitivity, genetic, and functional studies that have revolutionized the analysis of the set of nonessential genes (Giaever et al., 2002, 2004; Parsons et al., 2004).

Constructing an ESP Genetic-Interaction Map

We took advantage of the available functional and intracellular localization data to identify 424 genes (367 deletion strains of nonessential genes and 57 strains carrying DAmP alleles of essential ones) whose products are localized to, or impact on, the ESP (Balakrishnan et al., 2005; Huh et al., 2003; Kumar et al., 2002). By using cellular localization data derived from large-scale GFP fusion studies (Huh et al., 2003; Kumar et al., 2002) (for description of localizations used, see Table S2), we were able to include ~160 unknown or poorly characterized open reading frames (ORFs). To obtain an accurate and homogeneous functional nomenclature for our genes, we assigned each protein to a func-

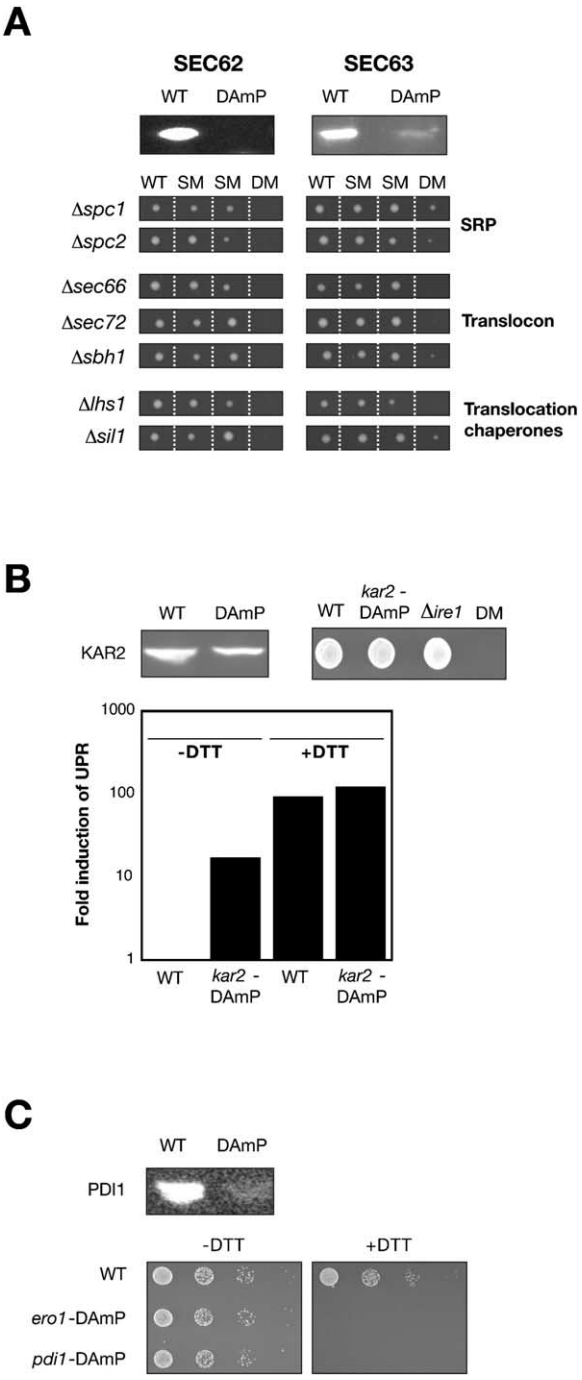

Figure 1. DAmP: A General Approach Producing Hypomorphic Alleles Suitable for Chemical and Genetic Analyses

(A) Upper panel: Western blots of the essential translocon component Sec62p and Sec63p levels in DAmP strains relative to wild-type (WT). Lower panel: tetrad analysis demonstrating aggravating genetic interactions between *sec62*- and *sec63*-DAmP and the indicated deletions in the nonessential signal recognition particle (SRP) proteins, translocon components, or translocation chaperones. Abbreviations used throughout: wild-type (wt), single mutants (SM), double mutants (DM).

(B) Upper left panel: Western blot of the essential chaperone Kar2p levels in DAmP strains relative to wt. Upper right panel: illustration of synthetic-lethal interaction between *kar2*-DAmP and a UPR-deficient strain (*Δire1*). Lower panel: UPR levels (normalized to untreated wt cells) in the indicated strains in the presence or absence of the reducing agent DTT. Note that *kar2*-DAmP strains induce the UPR; this in turn causes upregulation of *KAR2* transcription, which may explain the relatively low reduction in Kar2p levels in the DAmP strain.

(C) Upper panel: Western blot of Pdi1p levels in a DAmP strain relative to wt. Bottom panels: DTT sensitivity of *pdi1*-DAmP and *ero1*-DAmP (the two essential components of disulfide-bond formation in the ER) strains relative to wt. From left to right, the indicated strains are plated in 10-fold serial dilutions onto media containing or devoid of DTT.

tional category by reviewing the literature (Figure 2A and Table S2).

We developed a strategy for providing quantitative metrics of the strength of genetic interactions. Using the synthetic genetic array (SGA) approach (Tong et al., 2001), we generated double mutants for each of the genes in our ESP set. All double-mutant spores were plated under identical conditions, and colony sizes were measured by digital imaging (Parsons et al., 2004) (Figure 2B). In order to quantitatively evaluate both negative and positive epistatic relationships, we needed to compare the growth rate of each double mutant to that which would be expected given the growth rates of the two single mutants. One strategy for evaluating epistatic interactions would be to directly measure the growth rate of each single and double mutant and assume, as is typically done, that in the absence of an interaction the growth defect of a double mutant will be the product of the growth defects of the two single mutants (Phillips et al., 2000; Segre et al., 2005). However, uncertainty about the validity of this assumption as well the introduction of error associated with the measurement of single mutants makes this approach less desirable. Instead, we took advantage of the comprehensive nature of our data, and the fact that significant genetic interactions are rare, to empirically determine with high precision the expected size for each double mutant given its two mutations (S.R.C. and J.S.W., unpublished data). By comparing the observed colony sizes to these expected values, we obtained quantitative (Figure S1) measures for both negatively scored (aggravating) interactions, in which double mutants grow more slowly than expected, and positively scored (alleviating) interactions, where the double mutants grow more rapidly than expected (Figures 2B and 2C).

The quality of our data was greatly improved by the fact that each deletion was made independently with both antibiotic-resistance markers and both pairwise interactions were measured (Figure 2C). This 2-fold redundancy allowed us to identify incorrect strains (e.g., revertants or contaminants [~11% of the library]), which, along with strains that gave highly irreproducible results, we removed and, when practical, replaced. Having full biological replicates also eliminated many sources of systematic error. It further provided a direct measure of the experimental variability and allowed us to evaluate rigorously the significance of our measures as a function of the observed interaction score (S.R.C. and J.S.W., unpublished data) (Figure 2C, inset). In addition to allowing the evaluation of positive interactions,

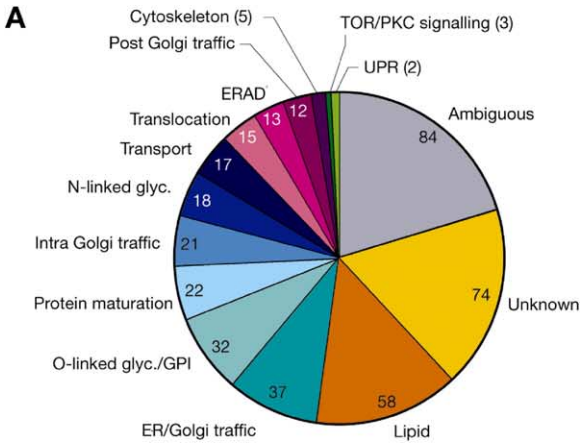

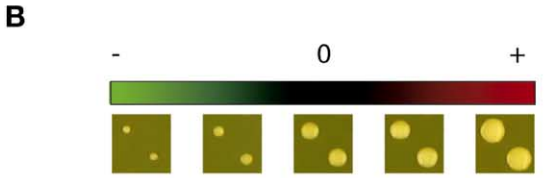

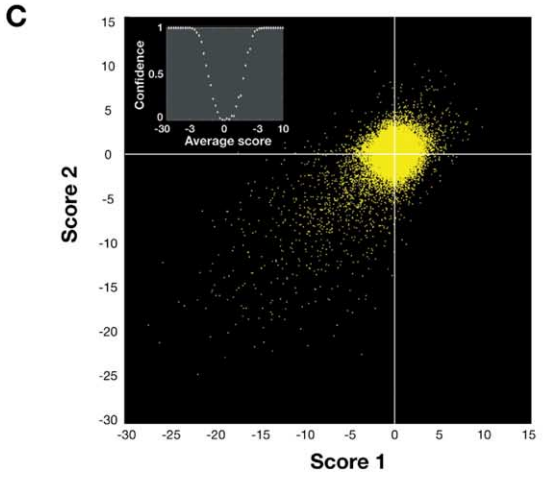

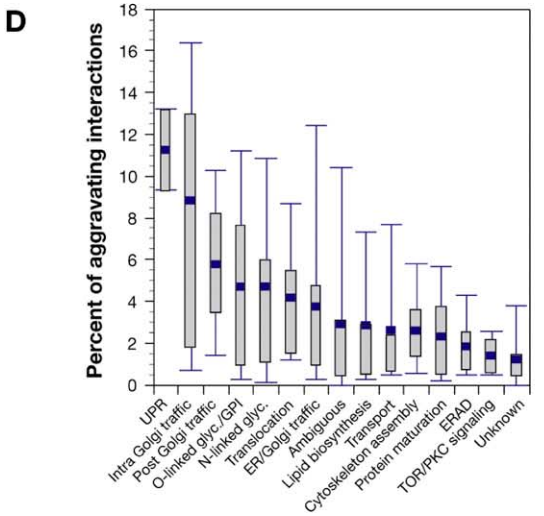

our quantitative metric provided a more sensitive approach than SGA or conventional tetrad analysis for detection of synthetic-lethal interactions (see Figure 2C, Figure S2A, and the UPR analysis below).

For most of the following analyses, we used a continuous score to describe interaction strength. However, where it was advantageous to have a discrete evaluation of interactions, we used a 95% confidence threshold (which corresponds to |score| > 2.5 [Figure 2C, inset]). Counting such significant interactions, we found that both the DAmP alleles of the essential and the deletions of nonessential genes, on average, showed SSL interactions with approximately 3% of this library, which is notably higher than the observed rate of 0.5% for the set of genome-wide SSL screens performed on the nonessential-deletion-mutant collection (Tong et al., 2004). Thus, by studying a dense, largely self-interacting set of genes, we obtained a high-confidence data set spanning a large fraction of each gene's interactions despite screening only a small fraction of possible gene pairs. Nonetheless, concentrating on a functional subset of genes means that some interactions will be missed, and therefore it would be advantageous to combine this approach with single-gene genome-wide screens.

The distribution of interactions varied widely for the different functional categories within the ESP, with UPR components having the highest mean number of interactions and uncharacterized ORFs having the lowest (Figure 2D). We selected the UPR category to evaluate experimentally the accuracy and completeness of our interaction measurements. Because deletion strains showing aggravating interactions with *IRE1* typically induce the UPR, we could assess the accuracy of our scoring independently of tetrad analysis. By measuring UPR activation using a fluorescent reporter, we confirmed that 34 of the 35 nonessential genes that were scored as having aggravating interactions with *IRE1* actually led to induction of the UPR. Analysis of the UPR data also argues for a low false-negative rate for

Figure 2. Overview of the Genetic-Interaction Map of the Early Secretory Pathway

(A) Distribution of early secretory pathway (ESP) gene functions analyzed and number of strains from each category (described in Table S3).

(B) Illustration of the range of colony sizes detected by the E-MAP strategy. The scale bar represents the color code used throughout the manuscript. No simple correspondence between score and colony size exists, as the interaction score also takes into account the growth defect of the single mutants.

(C) Scatter plot comparing independent interaction scores for each gene pair. Each point represents a single gene pair, with the two scores derived from independent measurements (each done in six replicates) in which the antibiotic-resistance gene (KAN or NAT) used to generate and mark the two gene deletions has been swapped. Inset is a graphic representation of the confidence value of interactions as a function of the average interaction score (S.R.C. and J.S.W., unpublished data).

(D) Distribution of significant aggravating interactions (>95% confidence, S < –2.5) for the strains of different functional groups. The blue box indicates the mean number of interactions. The gray box represents the 25th–75th percentile, and the bars indicate the 10th–90th percentile.

genetic interactions as only 4 of these 34 genes failed to show a significant interaction with the *IRE1*-dependant UPR inducer *HAC1* (Table S3).

Probing ESP Function Utilizing Hierarchical Clustering

Once quantitative measures of epistatic interactions have been obtained for each gene, the resulting pattern of scores can be regarded as a phenotypic signature. Hierarchical clustering (Eisen et al., 1998) of these signatures yielded a remarkably large number of functionally homogeneous subtrees (Figure 3). Perhaps even more notable was the ability of the clustering algorithm to make subtle distinctions within cellular processes, pointing to the high precision of the phenotypic signatures made possible by the comprehensive nature of the interaction data. This analysis also highlighted the value of obtaining quantitative data as well as data on positive interactions since the quality of the clusters deteriorated substantially when such information was not included (S.R.C. and J.S.W., unpublished data). To illustrate the depth of biological information in the genetic-interaction map, we present an interaction-dense area of the cluster (Figure 3A) and highlight five functionally homogeneous trees (entire cluster and raw data can be downloaded from the authors' website at http://phoibe.med.utoronto.ca/erg).

Cluster of N-Linked-Glycosylation Genes

This cluster consists exclusively of 11 well-characterized proteins dedicated to the generation of high-mannose chains. The cluster is further divided into two functionally distinct groups, one consisting of the ALG genes (involved in oligosaccharyl synthesis) and the other consisting of OST genes (involved in transfer of the sugar moiety onto nascent proteins). (See Figure 3B.)

Cluster of O-Linked-Glycosylation/GPI Biosynthesis Genes

Proximal to the N-linked glycosylation cluster are genes involved in O-linked glycosylation, GPI anchor biosynthesis, and other processes required for proper cell-wall formation (Lipke and Ovalle, 1998). Within this cluster are a number of functionally homogeneous subclusters, including that of *ROT2*, *CWH41*, and *CNE1*. These two glucosidases and a lectin chaperone mediate sugar trimming and subsequent recognition of N-linked glycans. The presence of these genes in this cluster, as opposed to the N-linked glycosylation cluster, reflects their role in maintaining integrity of the cell wall (Shahinian et al., 1998; Simons et al., 1998). Similarly, the presence of the Ca^{2+}/Mn^{2+} transporter, *PMR1*, may reflect its described role in Golgi-mediated carbohydrate modifications (Vashist et al., 2002). (See Figure 3C.)

Cluster of Posttranslational-Translocation Genes

This cluster includes five essential and nonessential core components of the posttranslational translocon. Significantly, these proteins are well distinguished from those involved in cotranslational translocation, which are found in a distinct subcluster. A sixth gene in this same cluster, *SPF1*, while not part of the translocation machinery, is known to contribute to establishing the correct orientation of transmembrane proteins during translocation (Tipper and Harley, 2002). (See Figure 3D.)

Cluster of Traffic Genes

This extensive cluster reveals multiple levels of functional organization. Globally, the distinct steps (ER/Golgi traffic, intra-Golgi traffic, and post-Golgi traffic) of vesicle transport were distinguished. Locally, there exists a high degree of functional structure (e.g., subtrees for the *RIC1/RGP1* heterodimer, the COG complex, and the AP-3 complex members [*APL5*, *APS3*, *APL6*, and *APM3*]). An intriguing subtree embedded within the ER/Golgi-traffic components consists of three poorly characterized genes, *MDM39*, *RMD7*, and *ARR4*, which we show to be in a physical complex involved in Golgi-to-ER traffic (see below). Thus, we propose that they be referred to as the GET complex. (See Figure 3E.)

Cluster of ER/Golgi-Traffic Genes

This cluster includes a subtree consisting of the heterotrimeric complex members *EMP24*, *ERV25*, and *ERP1* and three poorly characterized but highly conserved genes (*YEL043w*, *NNF2*, and *YIL039w*), which are strong candidates for novel components of the ER/Golgi-traffic machinery. (See Figure 3F.)

Predicting Physical Complexes and Pathways from Interaction Patterns

We next sought to use the genetic-interaction map to study more precisely the functional relationship among sets of genes. Each pair of genes is related by two distinct measures: the correlation between phenotypic signatures (as used for clustering) and the genetic-interaction score. We found that pairs of genes with intermediate levels of correlated phenotypic signatures were more likely to have negatively scored, aggravating interactions. However, as the degree of correlations grows, we see a striking reversal of this trend: the gene pairs with the most highly correlated signatures typically show no aggravating interactions and many even show positively scored interactions (Figure 4A). This behavior is precisely what might be expected for the deletion of proteins that act together in a coherent manner to perform a single function, as loss of any component would eliminate their common function. Thus, to identify proteins that act together (e.g., protein complexes and pathways), we devised an algorithm that calculates complex and pathway (COP) scores (S.R.C. and J.S.W., unpublished data) for finding sets of genes that are both highly correlated and lack an aggravating genetic interaction.

The top-scoring gene pairs included several sets of known complex or linear pathway components, as well as several predictions of novel ones. We focus below on five strongly scoring examples that demonstrate both complexes and pathways (for complete listing of scores, see Table S4). First is a linear signal-transduction pathway: the UPR sensor *IRE1* and its sole downstream effector *HAC1* (Figure 4B). Second is a biosynthetic pathway consisting of the ALG genes responsible for the sequential construction of high-mannose oligosaccharyl chains (Figure 4C). Third and fourth are dedicated protein complexes: the conserved oligomeric Golgi (COG) complex (Whyte and Munro, 2002) that functions in protein trafficking (Figure 4D) and the Ric1p/Rgp1p nucleotide exchange factor complex (Siniossoglou et al., 2000) (Figure 4E).

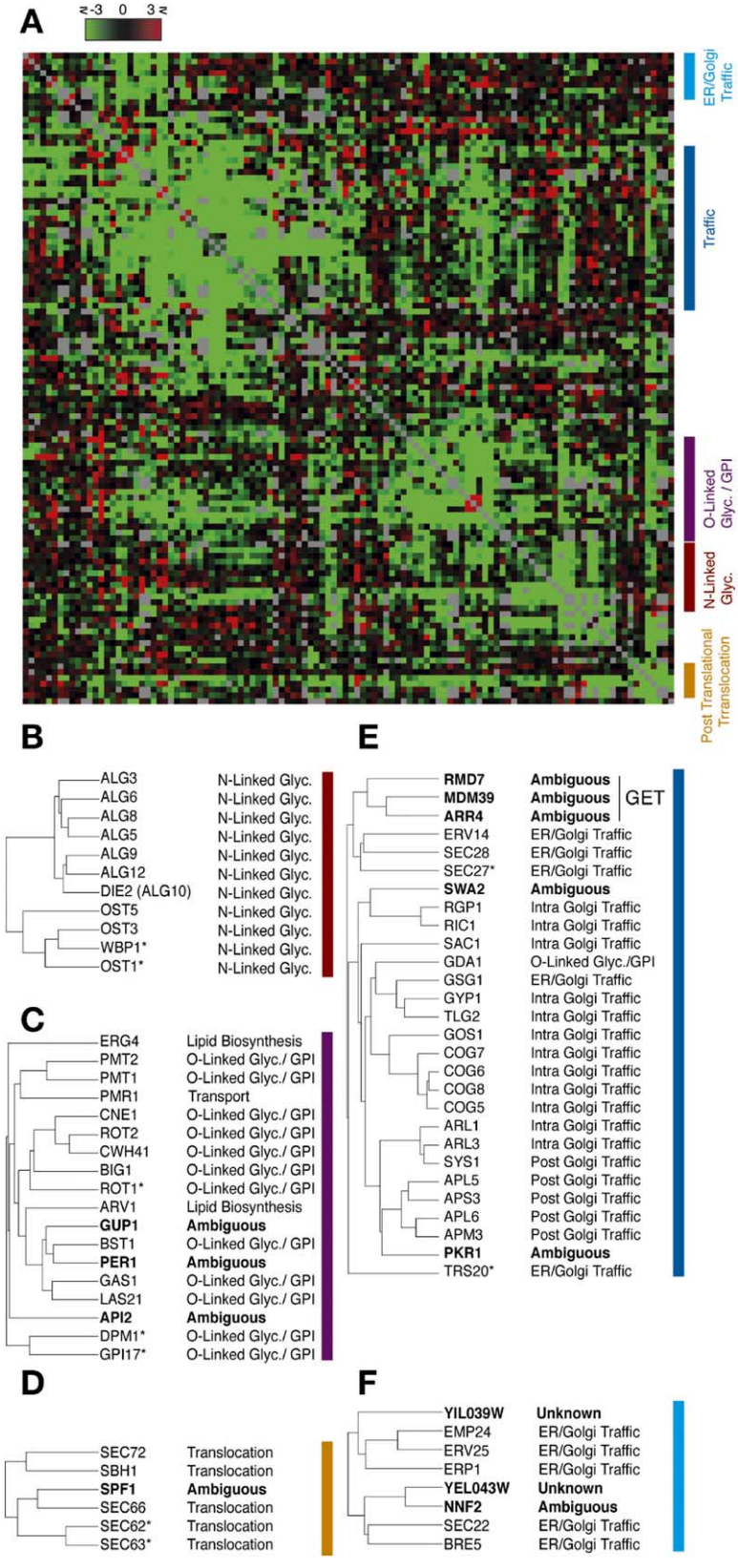

Figure 3. Hierarchical-Cluster Analysis of the ESP Genetic-Interaction Map

(A) A portion of the ESP cluster map. Each row/column represents the interaction pattern for a specific gene. Top left: color scale for interaction strength. Clustering is based on the degree of correlation between the pattern of genetic interaction of the various genes. Colored bars indicate functionally homogenous subclusters enlarged below.

(B–F) Bold lettering represents uncharacterized genes. Asterisks mark essential genes. The tree structure indicates the relative correlation of the different genes in a given cluster.

(B) N-linked glycosylation.

(C) O-linked glycosylation/GPI and other genes affecting cell-wall biosynthesis.

(D) Posttranslational translocation.

(E) General traffic. GET indicates a novel protein complex involved in *G*olgi-to-*E*R *t*raffic that is characterized below.

(F) ER/Golgi traffic.

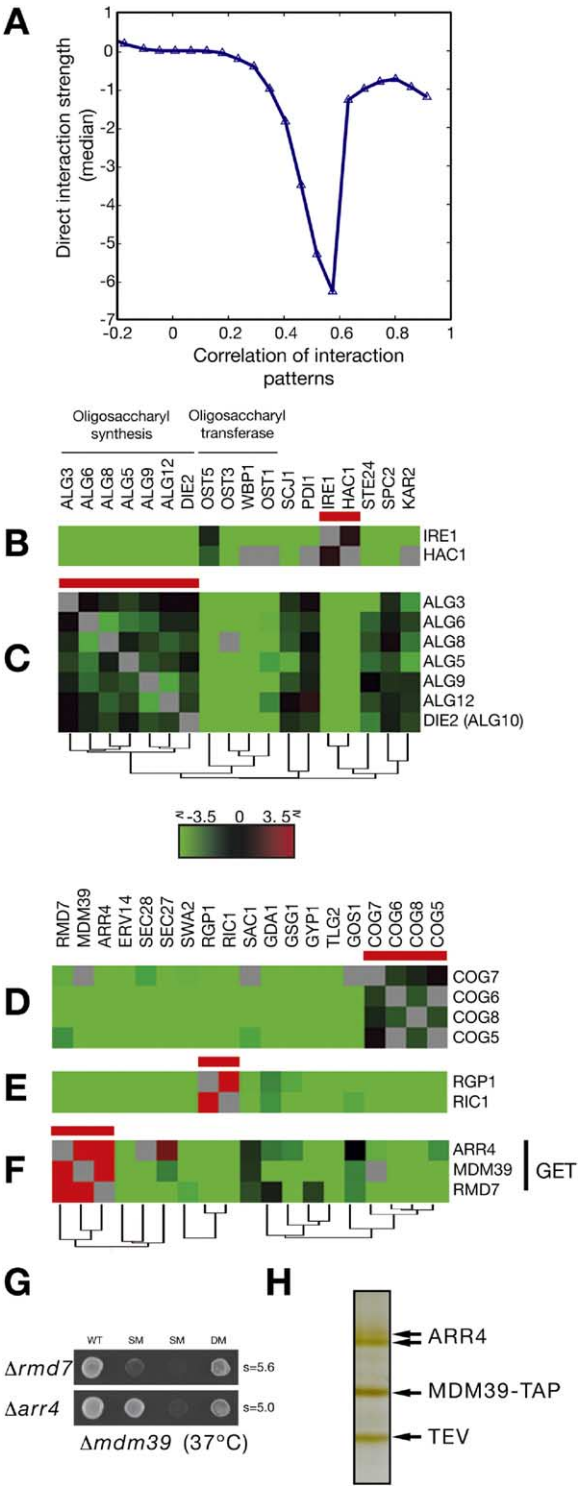

Figure 4. Complex and Pathways Predictions

(A) Plot of the median score for strength of direct genetic interaction between gene pairs as a function of the degree of correlation of their patterns of genetic interactions. Note that the most correlated gene pairs typically show little or no propensity to be involved in aggravating genetic interactions. This behavior is a signature of genes pairs that act together in a coherent fashion.

(B–F) Five examples of gene sets identified by use of the complex and pathways (COP) predicting algorithm that is based on the dual properties noted above. The red bar marks direct interactions. Trees as in Figure 3.

(B) *HAC1* and *IRE1*, which constitute the linear UPR pathway. Color scale as in Figure 3. Gray: no data.

(C) ALG genes responsible for the synthesis of precursors to N-linked glycosylation.

(D) Nonessential components of the COG complex.

(E) *RIC1*/*RGP1* exchange factor complex members.

(F) Newly identified GET complex members involved in retrieval of HDEL-containing proteins from the Golgi to the ER (See Figure 5).

(G) Suppressive interactions between GET complex members shown by growth of the indicated double mutant (DM) colonies at 37°C despite the temperature-sensitive phenotype of the *Δmdm39* (*Δget1*) mutation alone. This corroborates the positive-interaction score (S) observed for these genes.

(H) Affinity purification of MDM39p-TAP (Get1p-TAP), demonstrating physical interactions between Mdm39p (Get1p) and Arr4p (Get3p). A band resulting from the TEV protease is also indicated.

The final example is that of the three poorly characterized GET genes that were predicted from hierarchical clustering to be involved in ER/Golgi trafficking (Figure 4F). Some functional analyses of each of these proteins exist. However, these data, while not extensive, suggest that the GET complex proteins are actually involved in highly disparate functions. Mdm39p (Get1p) was suggested to play a role in mitochondrial biogenesis (Dimmer et al., 2002), Rmd7p (Get2p) was suggested to be involved in meiotic nuclear division (Enyenihi and Saunders, 2003), and Arr4p (Get3p) was implicated in arsenite transport (Shen et al., 2003). Nonetheless, our analysis shows these three genes to have highly similar patterns of epistatic interactions and strong positive genetic interactions between each other. These positive scores arise from suppression of the growth defect of *Δmdm39* (*Δget1*) by *Δarr4* (*Δget3*) and *Δrmd7* (*Δget2*) (Figure 4G). Taken together, these striking patterns of genetic interactions suggest that, despite the previous functional data, these three proteins are in fact functionally intimately related to each other. Consistent with this, affinity purification of TAP-tagged Mdm39p (Get1p) showed that it forms a robust complex with Arr4p (Get3p) (Figure 4H). Additionally, in large-scale analyses of protein complexes (Ho et al., 2002), Arr4p (Get3p) was suggested to interact with both Mdm39p (Get1p) and Rmd7p (Get2p), although another 33 physical interactions were also suggested for Arr4p (Get3p) (Gavin et al., 2002; Ho et al., 2002; Ito et al., 2001; Uetz et al., 2000), most of which are likely to be spurious.

Taken together, the above results illustrate how the high-density nature of the interaction data and the fact that both aggravating and alleviating interactions are quantified makes it is possible to identify sets of proteins acting together to carry out a single function. By contrast, many such relationships would not have been detected by conventional SSL analysis since it is often the case that strains carrying deletions in genes that act in concert with each other do not show synthetic interactions. More generally, the above analysis identifies one of many possible classes of epistatic relationships among gene sets, each of which would be indicative of a different class of functional relationship.

The GET Complex Is Required for Erd2p-Dependent Retrieval of HDEL Proteins to the ER

We chose to study the GET complex genes since the above analyses implicate them as constituting a protein complex involved in ER/Golgi traffic. Although *MDM39* (*GET1*) and *ARR4* (*GET3*) have clear mammalian homologs, little information on the specific function of these proteins can be discerned from their amino acid sequence alignments (Figure 5A). Consistent with the prediction that this complex functions in trafficking, we confirmed SSL interactions with traffic components by tetrad analysis (Figure S2A). Moreover, localization of the GFP-tagged proteins revealed that most of the GET complex shifted in its localization from the ER to punctate structures (which in part but not entirely colocalize with the Golgi marker *ANP1*; Huh et al., 2003; data not shown) when cells were shifted from growth in rich to minimal medium (Figure 5B). This shift of localization was dependent on the integrity of the complex since a deletion of the *MDM39* (*GET1*) gene caused Golgi retention of Arr4p-GFP (Get3p-GFP) (Figure 5B). Three independent assays using GET deletion strains, however, argued strongly against a role for the GET complex in anterograde trafficking: in GET deletion strains, the rate of maturation and export of the vacuolar protease CPY was unaffected (Figure S2B), localization of the putative ER to Golgi cargo receptor Emp47p (Sato and Nakano, 2002) was not altered (Figure S2C), and ER retention of the S11 invertase mutant (Bohni et al., 1987) was not compromised (Figure S2D).

What, then, is the role of the GET complex? Several observations indicate that it cooperates with Erd2p to mediate the ATP-dependent retrieval of resident ER proteins such as Kar2p and Pdi1p that contain the HDEL retrieval signal. First, the pattern of relocalization seen for GET complex proteins in response to media changes matches that of the Erd2p HDEL receptor (Figure 5B) (Semenza et al., 1990). Second, similarly to Arr4p-GFP (Get3p-GFP), the ER localization of Erd2p-GFP in rich media is dependent on *MDM39* (*GET1*) (Figure 5B). Third, deletion of any of the GET genes leads to strong secretion of HDEL proteins into the media (Figure 5C). This secretion phenotype was comparable to that seen for Kar2p lacking an HDEL signal (Figure 5C) and was UPR independent (Figure S2E), indicating that the HDEL retrieval system is strongly compromised in these strains. Fourth, secretion of Kar2p in the *ERD2* retrieval mutant (*erd2-b25*) (Semenza et al., 1990) was not further enhanced by deletions in GET complex members (Figure 5D), evidence that the role of the GET complex in HDEL retrieval is dependent on Erd2p. Finally, the function of the GET complex requires ATP hydrolysis since the G30R catalytically dead *ARR4* (*GET3*) mutant (Shen et al., 2003) failed to rescue the *ARR4* (*GET3*) deletion strain and in fact acts as a dominant negative (Figure 5C).

These observations suggest a model in which the GET complex functions to promote the ATP-dependent retrieval of the Erd2p HDEL receptor from the Golgi to the ER (Figure 5F). This model is consistent with an intriguing set of allele-specific genetic interactions between *ERD2* and *MDM39* (*GET1*): the *erd2-b25* allele suppresses the temperature-sensitive phenotype of *Δmdm39* (*Δget1*), while the *erd2*-DAmP hypomorphic allele is synthetically lethal with *Δmdm39* (*Δget1*) (Figure 5E). In the context of this model, if the *erd2-b25* mutation has a specific defect in interacting with the GET complex, then the mutant protein would not be sequestered by noncycling intermediates in the absence of Mdm39p (Get1p), causing suppression; conversely, reduced levels of Erd2p in the DAmP strain would aggravate the sequestration phenotype. Beyond the validity of this specific model, the distinct pattern of genetic interactions illustrates how defined hypomorphs for essential proteins can strongly complement partial loss of function alleles as tools for elucidating gene functions.

A Global View of Functional Organization within the ESP

A comprehensive genetic-interaction map not only provides precise information on individual genes but also generates genetic-interaction data on the level of functional modules. To reveal such information, we determined the number of observed genetic interactions between different functional modules and compared it to that expected by chance (S.R.C. and J.S.W., unpublished data) (Figure 6A). The resulting enrichment probability scores provide a portrait of interdependencies between the disparate functions that comprise the ESP (Figure 6B). The map faithfully recapitulates known relationships between ESP functions, such as the influence of the UPR on a wide range of secretory processes and the sequential dependence of each stage of vesicular trafficking on the previous one. It also reveals a strong connection between endoplasmic reticulum-associated degradation (ERAD) and lipid biosynthesis, the extent of which had not been previously well appreciated. E-MAPs thus provide a comprehensive and objective view of functional architecture that would be difficult to obtain using other methods.

Because each functional category showed a unique spectrum of interactions (Figure 6A), we could compare interaction patterns of specific strains to those of the functional categories to suggest biological roles for uncharacterized proteins (S.R.C. and J.S.W., unpublished data). We created an algorithm that predicted functions for the proteins in our library. Setting a threshold so that predictions were obtained for greater than 50% (83 total) of the poorly characterized or uncharacterized proteins in our data set, we observed 53% accuracy based on crossvalidation on annotated genes (For complete list of predictions, see Table S5). We tested these predictions for three genes whose function was not well defined by hierarchical clustering. The first protein, Ice2p, was only recently found in a screen for defects in cortical ER patterning (de Martin et al., 2005). Our algorithm predicted it would affect ERAD, and, indeed, its deletion led to stabilization of the well-characterized ERAD substrate CPY* (Figure 6C), although it is unclear whether this is a direct or indirect effect of its deletion.

Next we focused on *YDL099W*, an uncharacterized, early-Golgi-localized (Huh et al., 2003), coiled-coil protein. The spectrum of genetic interactions for YDL099W was most similar to that of the Golgi-localized protein Grh1p, and both were predicted to be involved in ER/

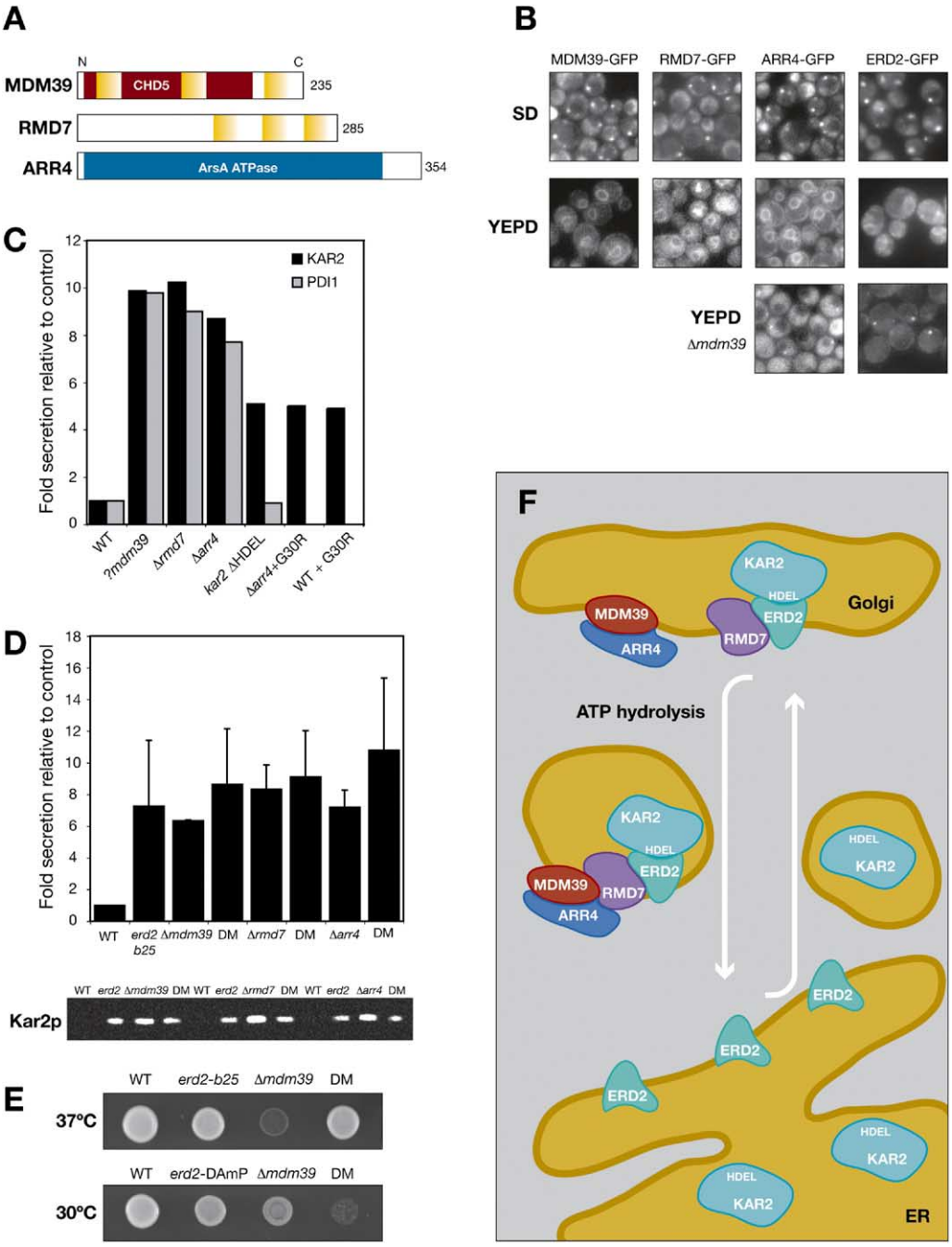

Figure 5. The GET Complex Is Required for the Erd2p-Dependent Retrieval of HDEL Proteins from the Golgi

(A) Schematic representation of the domain structure for the GET proteins. CHD5 is a coiled-coil domain. Yellow boxes represent putative transmembrane domains.

(B) Subcellular localization of GFP-tagged GET proteins and Erd2p in rich (YEPD) and synthetic media (SD). Bottom panels: localization of Arr4p (Get3p) and Erd2p in a *Δmdm39* (*Δget1*) strain in rich media.

(C) Effect of GET deletions on Kar2p and Pdi1p secretion. Also shown are Kar2p secretion levels caused by deletion of the HDEL retrieval signal (*kar2*-ΔHDEL) or expression of an ATPase-dead mutants (G30R) of *ARR4* (*GET3*) in a wild-type or *Δarr4* (*Δget3*) background.

(D) Effect of *erd2-b25* allele on Kar2p secretion alone or in combination with loss of GET members. Bottom panel: Western blot of secreted fraction. Top panel: quantitation of levels of secreted Kar2p. SD measurements from three independent experiments are shown.

(E) Genetic interactions between the *Δmdm39* (*Δget1*) strain and two different mutant *ERD2* alleles (*erd2-b25* and *erd2*-DAmP). Shown is growth of single and double mutants at the indicated temperatures. Note the opposite phenotype for the two alleles.

(F) Model for the ATP-dependent retrieval of Erd2p–HDEL complexes by the GET complex. Mdm39p (Get1p), Rmd7p (Get2p), and Arr4p (Get3p) are envisioned as promoting the retrieval from the Golgi to the ER of complexes between HDEL-containing proteins such as Kar2p and the HDEL receptor Erd2p. This retrieval function is dependent on the ATPase activity of Arr4p (Get3p).

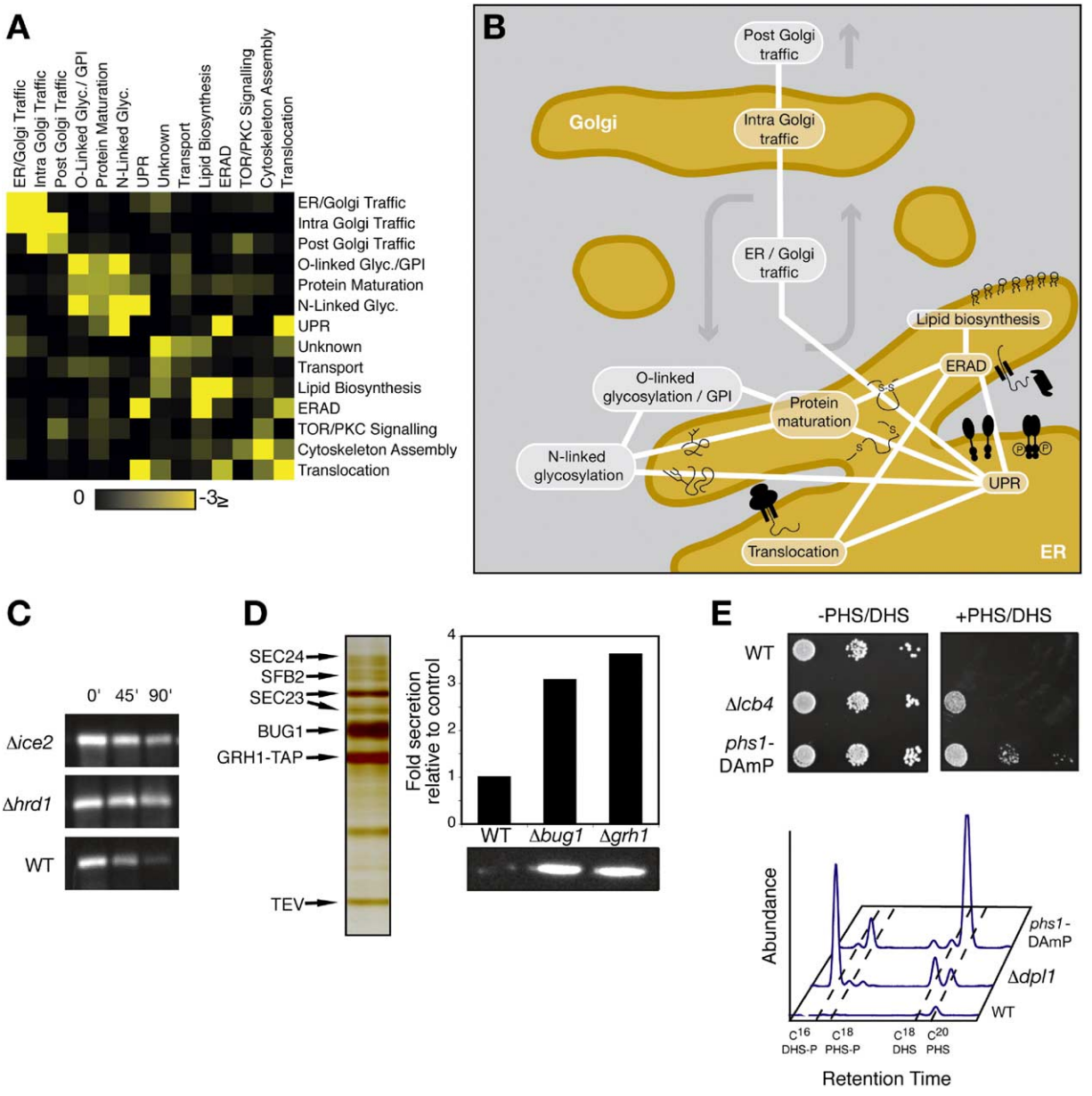

Figure 6. Genetic Interactions between Functional Modules Reveal Global ESP Structure and Allow Gene Discovery

(A) Matrix of enrichment probabilities for interactions ($\log_{10}$p-values) between functional categories (S.R.C. and J.S.W., unpublished data). Bottom: color scale.

(B) Schematic representation of interactions ($\log_{10} p \leq -0.5$) between different functional categories seen in (A).

(C) Effect of *Δice2* on ER-associated degradation (ERAD) as shown by kinetics of CPY* degradation. wt and *Δhrd1* (a well-characterized ERAD component) strains are shown for comparison.

(D) Effect of *Δbug1* and *Δgrh1* on Kar2p secretion (Bottom right: Western blot revealing secreted Kar2p; top right: quantitation of Kar2p secretion). Left panel: pulldown of Grh1p-TAP showing interaction with Bug1p and the indicated COPII components.

(E) Effect of *phs1*-DAmP on resistance to dihydrosphingosine (DHS) and phytosphingosine (PHS) relative to wild-type (WT) and the known DHS kinase *LCB4*. Bottom panel: HPLC chromatogram of the sphingolipid profile of *phs1*-DAmP. wt and *Δdpl1* (a known DHS lyase) chromatograms are shown for comparison. The identity of the characterized peaks is indicated.

Golgi traffic. *GRH1* has been implicated in the spindle assembly checkpoint, and its human homolog, *GRASP65*, is involved in Golgi reassembly during cell division (Norman et al., 1999; Sutterlin et al., 2002). We find the two proteins to be in a physical complex (Figure 6D, left panel) (this result was independently observed by F. Barr and S. Munro, who also observed an interaction with *USO1*; personal communication), and, based on these interactions, we propose that *YDL099W* be named *BUG1* (*b*inder of *USO1* and *GRH1*). Consistent with a role in ER/Golgi trafficking, deletion of *BUG1* or *GRH1* caused a UPR-independent Kar2p secretion

phenotype (Figure 6D, right panel). Moreover, Grh1p copurified with three members of the COPII vesicle coat (Sec23p, Sec24p, and Sfb2p) (Figure 6D, left panel). Taken together, these results support the predicted role of Bug1p and Grh1p in ER/Golgi trafficking and suggest a possible mechanistic link between Bug1p/Grh1p-mediated Golgi assembly and recruitment of ER-derived COPII vesicles.

The third example is the uncharacterized, essential, and highly conserved ORF, *YJL097W*, which our algorithm predicts to be involved in lipid biosynthesis. The set of genetic interactions of *yjl097w*-DAmP suggests a role in sphingolipid metabolism/signaling. For example, its strongest aggravating interaction is with a deletion in the phosphosphingosine phosphatase, *LCB3*, and its pattern of genetic interactions is most similar to that of a deletion in phosphosphingosine lyase, *DPL1*. We find that the DAmP allele of *YJL097W*, which we now name *PHS1* (*PTPLA h*omolog involved in sphingolipid biosynthesis 1), is highly resistant to external addition of both phytosphingosine (PHS) and dihydrosphingosine (DHS) (Figure 6E, top panel), as expected from a regulator of sphingosine levels. Chromatographic analysis of the sphingolipid contents of *phs1*-DAmP cells (Figure 6E, bottom panel) reveals a strong increase in a subset of cellular phosphosphingolipids. The mammalian homolog of *PHS1*, *PTPLA*, is a protein with unknown function that is highly expressed in developing cardiac tissue (Li et al., 2000). Phosphosphingosines are important for cardiac development in zebrafish (Kupperman et al., 2000), suggesting that *PTPLA* may play an important role in mammalian cardiac development.

Perspective

We have created a strategy for generating and analyzing quantitative, high-density genetic-interaction maps (E-MAPs) in yeast and have applied it to the early secretory pathway (ESP). We show that our genetic-interaction map contains an abundance of biological information. Our ability to extract precise functional information was dependent on two critical aspects of the E-MAP: the high-density nature of the data and the fact that both negative (aggravating) and positive (including buffering and suppressor) interactions are identified and quantified. Together these features made it possible, based solely on our epistatic data, to recapitulate known pathways within the ESP in detail and resolve closely related processes such as the different steps involved in the generation, transfer, and trimming of high-mannose glycans and the distinction between the post- and cotranslational translocation machinery. This argues that precise functional information can be inferred for genes of unknown function. Accordingly, many predictions have emerged from our analysis. Exploration of several of these allowed us to accurately identify novel, conserved components involved in extensively studied biological processes, including retrieval of HDEL proteins and sphingolipid biosynthesis.

Given the relative ease with which we generated these data, and given the ability of this approach to yield highly accurate predictions, extension of this strategy to other subsets of genes should provide a general tool for discovery of gene functions. While our ESP gene set was based largely on functional and localization data, a wide range of possible strategies for identifying related sets of genes for E-MAP analysis exists. This includes using transcriptional, protein-protein interaction and low-density SSL interaction data. Indeed, preliminary analysis of two additional interaction networks focusing on gene sets involved in transcription and DNA repair confirmed both the general feasibility and immediate value of constructing such interaction maps (unpublished data). Furthermore, once constructed, E-MAPs can act as a platform for further genetic-interaction studies since novel genes suspected of being involved in a process relevant to a particular E-MAP can be readily screened against that gene subset.

Beyond aiding in the cataloging of gene functions, the analysis of high-density interaction data provides a perspective on the organization of biological processes that is highly complementary to that obtained from existing genetic and biochemical approaches. For example, systematic genetic screens can now identify most proteins that impinge upon a biological process but do not indicate how direct that influence is. E-MAPs not only report on the spectrum of processes that are affected by loss of a given gene but further reveal the interdependency among them. This additional information helps distinguish direct from indirect effects, allowing a more complete understanding of the relationship between genotype and phenotype. Similarly, high-throughput biochemical approaches facilitate the systematic identification of physically interacting proteins. These can further be classified using the genetic-interaction data, which helps distinguish proteins that are involved in a single stable complex from those participating in multiple ones.

The fact that such an abundance of biological information could be derived from as simple a measure as relative growth provides strong motivation for future efforts to extend the construction of E-MAPs. An immediate goal is to improve the resolution of these maps by providing more precise quantitative measures of the relative fitness of the single versus double mutants, perhaps by modifying microarray-based approaches such as dSLAM (Pan et al., 2004), which make it possible to monitor the growth rate of many strains in parallel. An increase in precision would allow one to normalize the strength of epistatic interactions relative to the individual mutant defects (Segre et al., 2005) and thus to distinguish between different classes of pairwise epistatic relationships (e.g., buffering versus suppression). This, in turn, should greatly increase the ability to define functional relationships between gene products. Increased precision would also make it possible to assess directly the propensity of a gene to be involved in genetic interactions independently of the strength of its growth defect, allowing a rigorous evaluation of which genes represent genuine interaction hubs. The biological information obtained from such data could also be extended by measuring phenotypes other than growth rate using reporters that are sensitive to specific changes in cellular physiology. These experimental advances should also be accompanied by developing novel analytical approaches for extracting bio-

logical information. In concert with the above refinements, the E-MAP strategy could be implemented in more complex organisms, using RNAi or large-scale deletion libraries. Finally, high-density genetic-interaction maps could be used as tools for therapeutic discovery by examining synergistic interactions between gene depletions and drugs or drug pairs (Parsons et al., 2004).

The wealth of biological information yielded by our analysis of the ESP using the E-MAP approach, alongside the potential of genetic-interaction maps to be tailored to a wide variety of problems, argues that this strategy will provide a general framework for obtaining a more holistic understanding of complex biological systems.

Experimental Procedures

Media and Strains

Antibiotic-resistant strains were maintained in YEPD with either Geneticin (200 μg/ml) (GIBCO) or nourseothricin (NAT) (100 μg/ml) (Werner Bioagents). All drug assays were performed in SD media. Dithiothreitol (DTT) (Sigma) was used at 1 mM. Dihydrosphingosine/phytosphingosine (DHS/PHS) (BioMol) were used at 5 μM DHS or 20 μM PHS in 0.1% Tergitol (Sigma). See strain list in Table S6.

E-MAP Analysis

Growth and selection of double mutants were performed using SGA technology (Tong et al., 2001). Colony area was measured from digital images of the plates (Parsons et al., 2004). All analysis of the data (S.R.C. and J.S.W., unpublished data) was performed using MATLAB (The Mathworks, Natick, Massachusetts) and Excel. Clusters were made using the CLUSTER program (http://rana.lbl.gov/EisenSoftware.htm) and can be viewed by the JAVA TREEVIEW program (http://jtreeview.sourceforge.net/) (Eisen et al., 1998). Raw scores can be accessed at http://phoibe.med.utoronto.ca/erg or downloaded as a MATLAB file from the same website.

Immunoblotting

Western blots were performed as previously described (Semenza et al., 1990) with antisera against Kar2p, Sec62p, Sec63p (a kind gift from Peter Walter), or Pdi1p. For full description, see Supplemental Experimental Procedures.

Flow Cytometry Analysis

Mid-log cells in TE were analyzed using a LSR2 flow cytometer (Beckton Dickinson).

CPY* Degradation Assays

Degradation assays were performed as described (Bhamidipati et al., 2005). For full description, see Supplemental Experimental Procedures.

TAP Tagging and Mass Spectrometry

TAP-tagged proteins (Ghaemmaghami et al., 2003) were extracted with high-speed clarification, TAP purified, separated by 10% SDS-PAGE gels, visualized by silver staining, and identified by MALDI-TOF mass spectrometry (Krogan et al., 2002).

Microscopy

Live yeast expressing GFP fusions (Huh et al., 2003) were photographed using a fluorescent microscope (Axiovert 200M; Carl Zeiss MicroImaging, Inc.), a Cascade 512F CCD camera (Roper Scientific), and MetaMorph 6.2r6 acquisition software (Universal Imaging Corp.).

Plasmid Construction

Genomic region of *ARR4* (*GET3*) DNA was integrated into XhoI-cut p313. The ATPase-dead G30R mutation (Shen et al., 2003) was introduced using the QuikChange Site-Directed Mutagenesis Kit (Stratagene) and confirmed by DNA sequencing.

HPLC

Sphingolipid composition was analyzed as previously described (Lester and Dickson, 2001). For full description, see Supplemental Experimental Procedures.

Supplemental Data

Supplemental Data include Supplemental Experimental Procedures, seven tables, and two figures and can be found with this article online at http://www.cell.com/cgi/content/full/123/3/507/DC1/.

Acknowledgments

We thank M. Noble for help with strain construction; E. Kannegaard for help developing the DAmP system; J. Newman for help with FACS analysis; S. Munro and F. Barr for communicating results prior to publication; H. Ding, K. Vachon, L. Le, C. Sun, K. Chin, Z. Hassam, X. Wu, M. Lim, T. Chan, J. Rilestone, and K. Takhar for help with screens; Affinium Pharmaceuticals for mass spectrometry; R. Parker for helpful discussions regarding the DAmP strategy; F. Winston, J. Ingles, K. Tipton, S. Ghaemmaghami, D. Cameron, and O. Schuldiner for discussions and critical reading of the manuscript; and A. DePace for help with graphics. We would like to thank H. Dieter Schmitt, P. Walter, and M. Rose for reagents. This work was supported by funds from HHMI (J.S.W.), the HFSP (M.S.), the Burroughs Wellcome Foundation (S.R.C.), the Ontario Genomics Institute and Genome Canada (J.F.G., B.A., and C.B.), and the CIHR (C.B., N.J.K., and B.A.).

Received: July 12, 2005
Revised: August 12, 2005
Accepted: August 22, 2005
Published: November 3, 2005

References

Balakrishnan, R., Christie, K.R., Costanzo, M.C., Dolinski, K., Dwight, S.S., Engel, S.R., Fisk, D.G., Hirschman, J.E., Hong, E.L., Nash, R., et al. (2005). Fungal BLAST and model organism BLASTP best hits: New comparison resources at the Saccharomyces Genome Database (SGD). Nucleic Acids Res. *33*, D374–D375.

Bhamidipati, A., Denic, V., Quan, E.M., and Weissman, J.S. (2005). Exploration of the topological requirements of ERAD identifies Yos9p as a lectin sensor of misfolded glycoproteins in the ER lumen. Mol. Cell *19*, 741–751.

Bohni, P.C., Schauer, I., Tekamp-Olson, P., and Schekman, R. (1987). Signal peptide cleavage mutants of yeast invertase. In Proteases and Biological Control and Technology (New York: Oxford University Press), pp. 255–264.

de Martin, P.E., Du, Y., Novick, P., and Ferro-Novick, S. (2005). Ice2p is important for the distribution and structure of the cortical ER network in Saccharomyces cerevisiae. J. Cell Sci. *118*, 65–77.

Dimmer, K.S., Fritz, S., Fuchs, F., Messerschmitt, M., Weinbach, N., Neupert, W., and Westermann, B. (2002). Genetic basis of mitochondrial function and morphology in Saccharomyces cerevisiae. Mol. Biol. Cell *13*, 847–853.

Eisen, M.B., Spellman, P.T., Brown, P.O., and Botstein, D. (1998). Cluster analysis and display of genome-wide expression patterns. Proc. Natl. Acad. Sci. USA *95*, 14863–14868.

Elena, S.F., and Lenski, R.E. (1997). Test of synergistic interactions among deleterious mutations in bacteria. Nature *390*, 395–398.

Enyenihi, A.H., and Saunders, W.S. (2003). Large-scale functional genomic analysis of sporulation and meiosis in Saccharomyces cerevisiae. Genetics *163*, 47–54.

Gavin, A.C., Bosche, M., Krause, R., Grandi, P., Marzioch, M., Bauer, A., Schultz, J., Rick, J.M., Michon, A.M., Cruciat, C.M., et al. (2002). Functional organization of the yeast proteome by systematic analysis of protein complexes. Nature *415*, 141–147.

Ghaemmaghami, S., Huh, W.K., Bower, K., Howson, R.W., Belle, A., Dephoure, N., O'Shea, E.K., and Weissman, J.S. (2003). Global analysis of protein expression in yeast. Nature *425*, 737–741.

Giaever, G., Chu, A.M., Ni, L., Connelly, C., Riles, L., Veronneau, S., Dow, S., Lucau-Danila, A., Anderson, K., Andre, B., et al. (2002). Functional profiling of the Saccharomyces cerevisiae genome. Nature *418*, 387–391.

Giaever, G., Flaherty, P., Kumm, J., Proctor, M., Nislow, C., Jaramillo, D.F., Chu, A.M., Jordan, M.I., Arkin, A.P., and Davis, R.W. (2004). Chemogenomic profiling: identifying the functional interactions of small molecules in yeast. Proc. Natl. Acad. Sci. USA *101*, 793–798.

Ho, Y., Gruhler, A., Heilbut, A., Bader, G.D., Moore, L., Adams, S.L., Millar, A., Taylor, P., Bennett, K., Boutilier, K., et al. (2002). Systematic identification of protein complexes in Saccharomyces cerevisiae by mass spectrometry. Nature *415*, 180–183.

Hughes, T.R., Marton, M.J., Jones, A.R., Roberts, C.J., Stoughton, R., Armour, C.D., Bennett, H.A., Coffey, E., Dai, H., He, Y.D., et al. (2000). Functional discovery via a compendium of expression profiles. Cell *102*, 109–126.

Huh, W.K., Falvo, J.V., Gerke, L.C., Carroll, A.S., Howson, R.W., Weissman, J.S., and O'Shea, E.K. (2003). Global analysis of protein localization in budding yeast. Nature *425*, 686–691.

Ito, T., Chiba, T., Ozawa, R., Yoshida, M., Hattori, M., and Sakaki, Y. (2001). A comprehensive two-hybrid analysis to explore the yeast protein interactome. Proc. Natl. Acad. Sci. USA *98*, 4569–4574.

Kelley, R., and Ideker, T. (2005). Systematic interpretation of genetic interactions using protein networks. Nat. Biotechnol. *23*, 561–566.

Krogan, N.J., Kim, M., Ahn, S.H., Zhong, G., Kobor, M.S., Cagney, G., Emili, A., Shilatifard, A., Buratowski, S., and Greenblatt, J.F. (2002). RNA polymerase II elongation factors of Saccharomyces cerevisiae: a targeted proteomics approach. Mol. Cell. Biol. *22*, 6979–6992.

Kumar, A., Agarwal, S., Heyman, J.A., Matson, S., Heidtman, M., Piccirillo, S., Umansky, L., Drawid, A., Jansen, R., Liu, Y., et al. (2002). Subcellular localization of the yeast proteome. Genes Dev. *16*, 707–719.

Kupperman, E., An, S., Osborne, N., Waldron, S., and Stainier, D.Y. (2000). A sphingosine-1-phosphate receptor regulates cell migration during vertebrate heart development. Nature *406*, 192–195.

Lester, R.L., and Dickson, R.C. (2001). High-performance liquid chromatography analysis of molecular species of sphingolipid-related long chain bases and long chain base phosphates in Saccharomyces cerevisiae after derivatization with 6-aminoquinolyl-N-hydroxysuccinimidyl carbamate. Anal. Biochem. *298*, 283–292.

Li, D., Gonzalez, O., Bachinski, L.L., and Roberts, R. (2000). Human protein tyrosine phosphatase-like gene: expression profile, genomic structure, and mutation analysis in families with ARVD. Gene *256*, 237–243.

Lipke, P.N., and Ovalle, R. (1998). Cell wall architecture in yeast: new structure and new challenges. J. Bacteriol. *180*, 3735–3740.

Mnaimneh, S., Davierwala, A.P., Haynes, J., Moffat, J., Peng, W.T., Zhang, W., Yang, X., Pootoolal, J., Chua, G., Lopez, A., et al. (2004). Exploration of essential gene functions via titratable promoter alleles. Cell *118*, 31–44.

Muhlrad, D., and Parker, R. (1999). Aberrant mRNAs with extended 3′ UTRs are substrates for rapid degradation by mRNA surveillance. RNA *5*, 1299–1307.

Norman, T.C., Smith, D.L., Sorger, P.K., Drees, B.L., O'Rourke, S.M., Hughes, T.R., Roberts, C.J., Friend, S.H., Fields, S., and Murray, A.W. (1999). Genetic selection of peptide inhibitors of biological pathways. Science *285*, 591–595.

Pan, X., Yuan, D.S., Xiang, D., Wang, X., Sookhai-Mahadeo, S., Bader, J.S., Hieter, P., Spencer, F., and Boeke, J.D. (2004). A robust toolkit for functional profiling of the yeast genome. Mol. Cell *16*, 487–496.

Parsons, A.B., Brost, R.L., Ding, H., Li, Z., Zhang, C., Sheikh, B., Brown, G.W., Kane, P.M., Hughes, T.R., and Boone, C. (2004). Integration of chemical-genetic and genetic interaction data links bioactive compounds to cellular target pathways. Nat. Biotechnol. *22*, 62–69.

Patil, C., and Walter, P. (2001). Intracellular signaling from the endoplasmic reticulum to the nucleus: the unfolded protein response in yeast and mammals. Curr. Opin. Cell Biol. *13*, 349–355.

Phillips, P.C., Otto, S.P., and Whitlock, M.C. (2000). Beyond the average: the evolutionary importance of gene interactions and variability of epistatic effects. In Epistasis and the Evolutionary Process, J.B. Wolf, E.D. Brodie, and M.J. Wade, eds. (New York: Oxford University Press), pp. 20–38.

Sato, K., and Nakano, A. (2002). Emp47p and its close homolog Emp46p have a tyrosine-containing endoplasmic reticulum exit signal and function in glycoprotein secretion in Saccharomyces cerevisiae. Mol. Biol. Cell *13*, 2518–2532.

Segre, D., Deluna, A., Church, G.M., and Kishony, R. (2005). Modular epistasis in yeast metabolism. Nat. Genet. *37*, 77–83.

Semenza, J.C., Hardwick, K.G., Dean, N., and Pelham, H.R. (1990). ERD2, a yeast gene required for the receptor-mediated retrieval of luminal ER proteins from the secretory pathway. Cell *61*, 1349–1357.

Shahinian, S., Dijkgraaf, G.J., Sdicu, A.M., Thomas, D.Y., Jakob, C.A., Aebi, M., and Bussey, H. (1998). Involvement of protein N-glycosyl chain glucosylation and processing in the biosynthesis of cell wall beta-1,6-glucan of Saccharomyces cerevisiae. Genetics *149*, 843–856.

Shen, J., Hsu, C.M., Kang, B.K., Rosen, B.P., and Bhattacharjee, H. (2003). The Saccharomyces cerevisiae Arr4p is involved in metal and heat tolerance. Biometals *16*, 369–378.

Simons, J.F., Ebersold, M., and Helenius, A. (1998). Cell wall 1,6-beta-glucan synthesis in Saccharomyces cerevisiae depends on ER glucosidases I and II, and the molecular chaperone BiP/Kar2p. EMBO J. *17*, 396–405.

Siniossoglou, S., Peak-Chew, S.Y., and Pelham, H.R. (2000). Ric1p and Rgp1p form a complex that catalyses nucleotide exchange on Ypt6p. EMBO J. *19*, 4885–4894.

Sutterlin, C., Hsu, P., Mallabiabarrena, A., and Malhotra, V. (2002). Fragmentation and dispersal of the pericentriolar Golgi complex is required for entry into mitosis in mammalian cells. Cell *109*, 359–369.

Tipper, D.J., and Harley, C.A. (2002). Yeast genes controlling responses to topogenic signals in a model transmembrane protein. Mol. Biol. Cell *13*, 1158–1174.

Tong, A.H., Evangelista, M., Parsons, A.B., Xu, H., Bader, G.D., Page, N., Robinson, M., Raghibizadeh, S., Hogue, C.W., Bussey, H., et al. (2001). Systematic genetic analysis with ordered arrays of yeast deletion mutants. Science *294*, 2364–2368.

Tong, A.H., Lesage, G., Bader, G.D., Ding, H., Xu, H., Xin, X., Young, J., Berriz, G.F., Brost, R.L., Chang, M., et al. (2004). Global mapping of the yeast genetic interaction network. Science *303*, 808–813.

Tu, B.P., and Weissman, J.S. (2004). Oxidative protein folding in eukaryotes: mechanisms and consequences. J. Cell Biol. *164*, 341–346.

Uetz, P., Giot, L., Cagney, G., Mansfield, T.A., Judson, R.S., Knight, J.R., Lockshon, D., Narayan, V., Srinivasan, M., Pochart, P., et al. (2000). A comprehensive analysis of protein-protein interactions in Saccharomyces cerevisiae. Nature *403*, 623–627.

Vashist, S., Frank, C.G., Jakob, C.A., and Ng, D.T. (2002). Two distinctly localized p-type ATPases collaborate to maintain organelle homeostasis required for glycoprotein processing and quality control. Mol. Biol. Cell *13*, 3955–3966.

Whyte, J.R., and Munro, S. (2002). Vesicle tethering complexes in membrane traffic. J. Cell Sci. *115*, 2627–2637.